

SKIP: Sparse Keyframe Interpolation Paradigm for Efficient Embodied World Models

Ziheng He^{1,2}, Yixiang Chen^{1,2}, Ning Yang^{1,3}, Zhanqian Wu⁴, Qisen Ma^{1,2}, Yuan Xu^{1,2},
Jiabing Yang^{1,2}, Peiyan Li^{1,2}, Xiangnan Wu^{1,2}, Xiaofeng Wang^{4,5}, Zheng Zhu^{4,5}, Jing Liu⁶,
Nianfeng Liu⁶, Yan Huang^{1,2,6,*}

¹UCAS ²CASIA ³NJU ⁴GigaAI ⁵THU ⁶FiveAges
heziheng261@mails.ucas.ac.cn

Abstract: Embodied world models have emerged as a promising paradigm in robotics by predicting how robot actions affect the surrounding scene. However, the rollout inference remains computationally expensive in pixel space, as long-horizon manipulation videos typically have to be generated frame by frame. This cost cannot be easily reduced by indiscriminately dropping frames, since downstream policies rely on complete preservation of sparse task-relevant events such as approach, contact, grasp, and release. To address this challenge, we propose Sparse Keyframe Interpolation Paradigm (SKIP), an event-preserving sparse-to-dense framework that avoids dense frame-by-frame generation. SKIP first identifies task-relevant keyframes by leveraging robot-aware multimodal features. It then synthesizes only these keyframes with a sparse video diffusion model. A learned gap predictor and an action-conditioned interpolator subsequently reconstruct the missing intervals according to the robot actions. On LIBERO, SKIP generates dense rollouts $4.16\times$ faster than a dense baseline while improving visual fidelity and reducing aggregate FVD by 89.0%. Importantly, SKIP-generated videos are effective policy-training data. Even when they fully replace real demonstrations, $\pi_{0.5}$ success drops only 1.3 pp in LIBERO simulation and 6.7 pp on the real robot, whereas fully dense frame-by-frame generation collapses by 48 to 58 pp.

Keywords: Embodied World Models, Keyframe-Based Video Generation, Robot Manipulation

1 Introduction

Recent Vision-Language-Action (VLA) models have achieved rapid progress in robot manipulation [1, 2, 3, 4, 5, 6, 7]. However, their performance still depends heavily on large-scale robot demonstrations for training and on real-world trials for behavior validation. As both are costly and time-consuming, there is strong motivation to develop embodied world models capable of predicting how candidate robot actions unfold in a given scene. Such predictions can both supply synthetic training data and verify behavior without real-world execution. In particular, generative video world models make these predictions explicit as pixel-level rollouts.

However, this explicitness usually requires high inference cost, because current generative video world models [8, 9, 10, 11] typically implement diffusion computation frame by frame. It is redundant since most neighboring frames contain similar backgrounds and manipulator-motion patterns. A straightforward alternative is temporal sparsification, explored in video summarization [12, 13], temporal action localization [14, 15], and hierarchical video generation [16, 17]. However, the criteria for selecting keyframes in these areas are quite different from what embodied manipulation requires.

* Corresponding author.

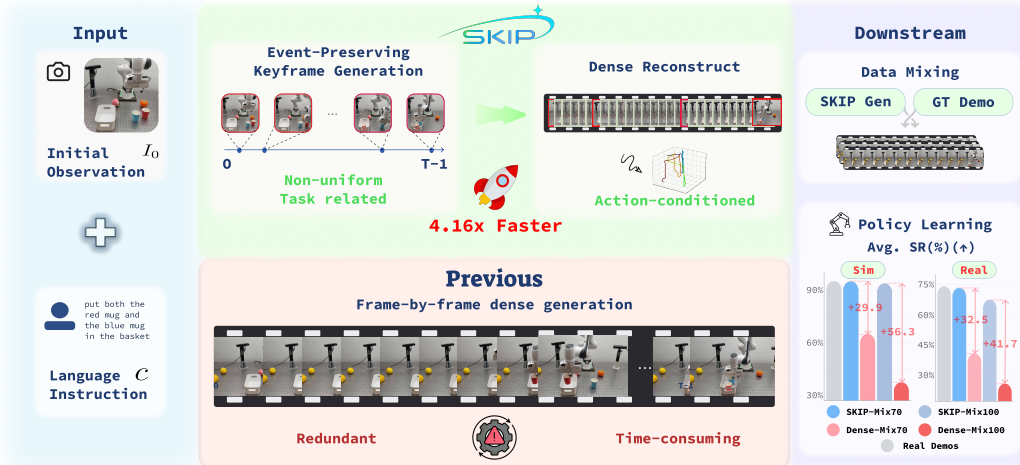


Figure 1: **Overview of SKIP.** Our framework predicts event-preserving sparse keyframes from an initial observation and a language instruction, then recovers the dense rollout via learned gap prediction and action-conditioned interpolation.

For example, in a fixed-camera manipulation rollout, where usually only the robot arm and the manipulated object move, the task-relevant information concentrates at a few discrete events such as an approach end, a gripper closing, a contact, or a release. These events are separated by smooth free-space motion that is visually near-redundant and similar in motion patterns, which is exactly where uniform sampling and generic-video criteria become misaligned. The difficulty of interpolation also varies significantly across frames. Dropping even a few frames during a gripper closure can miss the critical moment that determines whether the rollout successfully grasps the object. These frames often exhibit only a few pixels of visual change, making their loss abrupt and unrecoverable. Preserving these events is therefore essential, yet generic sparse-video methods ignore this embodiment-specific structure and routinely drop them.

To address this gap, we propose SKIP, an event-preserving sparse-to-dense framework for efficient explicit rollout inference in generative video world models. As illustrated in Figure 1, SKIP decouples dense rollout synthesis into two phases, event-preserving keyframe generation and dense reconstruction, realized by three modules. SKIP-SELECTOR identifies event-preserving keyframes through robot-aware multimodal fusion, which supervise SKIP-GENERATOR to synthesize only these keyframes. SKIP-RECONSTRUCTOR then recovers the dense rollout with a learned gap predictor and an action-conditioned interpolator. At inference, only SKIP-GENERATOR and SKIP-RECONSTRUCTOR run, realizing the two phases and producing dense action-aligned rollouts ready for downstream policy training and behavior-level inspection.

Our contributions are summarized as follows. **(1)** We show that a few decisive manipulation events can largely replace dense frame-by-frame generation, supporting both policy training and behavior preview. **(2)** We realize this paradigm as SKIP, in which SKIP-SELECTOR selects event-preserving keyframes through robot-aware multimodal fusion, SKIP-GENERATOR synthesizes only these keyframes, and SKIP-RECONSTRUCTOR recovers the dense action-aligned rollout via learned gap prediction and action-conditioned interpolation. **(3)** On LIBERO [18], SKIP runs $4.16\times$ faster than a dense baseline with higher fidelity. Moreover, even fully replacing real demonstrations for $\pi_{0.5}$ [6] training drops success by only 1.3 pp in LIBERO simulation and 6.7 pp on a four-task Franka real robot, versus a 48 to 58 pp collapse for fully dense-generated rollouts.

2 Related Work

Embodied world models. Embodied world models (EWMs) predict how candidate robot actions unfold in the environment, supporting policy learning, planning, and behavior inspection. Latent or embedding-space EWMs such as Dreamer [19, 20], TD-MPC2 [21], and V-JEPA [22, 23] roll out in compact internal states. These are efficient for control but inaccessible for pixel-level inspection or VLA training. Generative video EWMs such as IRASim [24] synthesize explicit pixel rollouts directly usable for policy learning and inspection, but their dense frame-by-frame generation makes inference time-consuming for long manipulation trajectories. A related line of work scales robot data without new teleoperation through simulation, replay, or augmentation [25, 26, 27], reshaping how data is constructed but leaving the per-rollout generative cost untouched. SKIP instead targets this per-rollout cost, decoupling sparse keyframe synthesis from lightweight action-guided recovery to keep pixel-level rollouts while removing redundant frame-by-frame computation.

Keyframe extraction and event preservation. Keyframe extraction is widely used to reduce temporal redundancy in video summarization [12, 13], temporal action localization [14, 15], and hierarchical video generation [16, 17], but these criteria are misaligned with manipulation’s event-driven structure. The underlying sparse-to-dense principle is also effective in adjacent generative domains such as human motion diffusion [28], but has not been adapted to action-conditioned embodied video world models. The closest robot-specific efforts still select keyframes at a coarse, single-modality level. KeyWorld [29] uses pose-only RDP simplification, and RoboEnvision [30] uses language-defined subtask boundaries with visual-only interpolation. SKIP instead selects fine-grained physical events through robot-aware multimodal fusion and validates the generated keyframe videos as a substitute for real demonstrations in both simulation and on a real robot.

Action-conditioned dense reconstruction. Recovering continuous video from sparse frames is a standard generative task, but embodied AI requires the recovered intermediates to align with robot actions. Generic frame interpolation [31, 32, 33] is efficient but action-agnostic, failing to model variable pauses or gripper-state changes when relying on visual endpoints alone. Action-conditional video prediction [34, 35, 36] captures action dynamics but defaults to dense, frame-by-frame generation. SKIP addresses this trade-off with a lightweight action-guided interpolator that fuses visual anchors with continuous action sequences to maintain tight action alignment without the dense diffusion overhead.

3 SKIP

3.1 Problem formulation and overview

Our objective is an efficient video world model that simulates how candidate robot actions unfold in the physical world, using a dataset of expert demonstrations for downstream planning, behavior validation, and policy training. Each demonstration $\tau = (\mathcal{I}, \mathcal{A}, \mathcal{S}, c)$ consists of an RGB observation sequence $\mathcal{I} = \{I_t\}_{t=0}^{T-1}$, an expert action sequence $\mathcal{A} = \{\mathbf{a}_t\}_{t=0}^{T-2}$, an optional proprioceptive stream $\mathcal{S} = \{\mathbf{s}_t\}_{t=0}^{T-1}$, and a language instruction c . Given the initial observation I_0 , the language instruction c , and the future actions \mathcal{A} , our model predicts the future RGB observations $\hat{\mathcal{I}}_{1:T-1}$, where $\hat{\cdot}$ marks model-generated quantities throughout.

SKIP consists of three modules (Figure 2): SKIP-SELECTOR, SKIP-GENERATOR, and SKIP-RECONSTRUCTOR, detailed in the following subsections.

3.2 SKIP-SELECTOR and SKIP-GENERATOR: Event-preserving keyframe generation

Keyframe selection criteria designed for generic video tasks are not well-suited to embodied manipulation. Content-agnostic and feature-clustering heuristics ignore the event-driven temporal structure of manipulation rollouts, while the closest robot-specific criterion, pose-only geometric simplification [29], depends on full proprioception that is often unavailable in video-only datasets and overlooks visual events with a small pose signature.

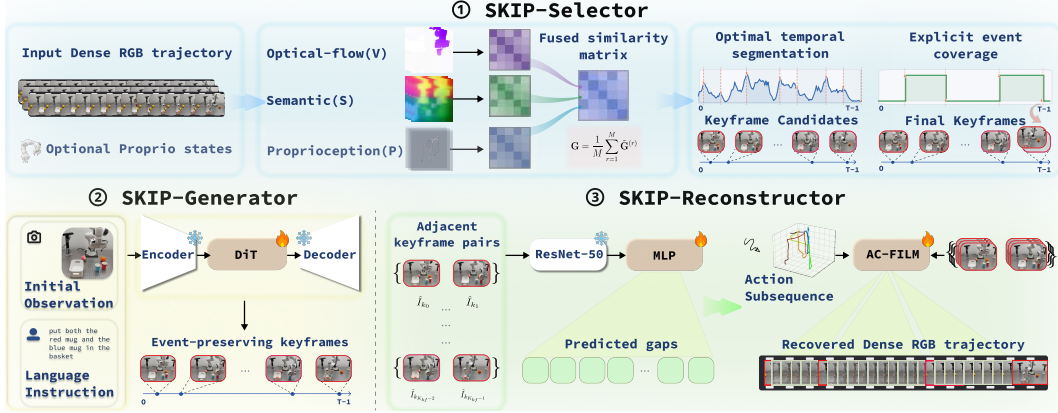


Figure 2: **SKIP architecture.** **SKIP-SELECTOR:** fuses visual, semantic, and optional proprioceptive features into similarity matrices, applies temporal segmentation, and enforces gripper-event coverage to yield a sparse set of event-preserving keyframes. **SKIP-GENERATOR:** a fine-tuned video diffusion model synthesizes only these keyframes from the initial observation and language instruction. **SKIP-RECONSTRUCTOR:** at synthesis time a gap predictor estimates the temporal gap between successive generated keyframes, and an action-conditioned interpolator runs over the corresponding action subsequences to reconstruct a dense rollout for policy training.

Motivated by these task-specific demands, we introduce SKIP-SELECTOR. As depicted in the top panel of Figure 2, SKIP-SELECTOR processes the dense RGB trajectory alongside an optional proprioceptive stream to output a sparse keyframe index set \mathcal{K} of user-configurable size K_{kf} . Each frame is represented by three complementary streams: optical-flow features (V) for dense manipulator motion, frozen DINO features (S) [37, 38] for semantic scene changes, and optional proprioceptive features (P) for contact events invisible to vision.

Robot-aware similarity fusion. We fuse these heterogeneous streams into a unified similarity representation. Direct feature concatenation would allow high-dimensional streams to dominate low-dimensional signals in the distance metric. To address this imbalance, we compute an independent RBF kernel matrix [39] for each available modality r : $G_{ij}^{(r)} = \exp(-\|\mathbf{f}_i^{(r)} - \mathbf{f}_j^{(r)}\|^2 / (2\sigma_r^2))$ measures the similarity between frames i and j , with σ_r set to the median pairwise distance. We then center and trace-normalize each modality matrix before averaging them into a fused similarity matrix $\mathbf{G} = \frac{1}{M} \sum_{r=1}^M \mathbf{G}^{(r)}$, where M is the number of available modalities. This fusion constrains each modality within its own geometry and allows all feature streams to contribute comparably.

Optimal temporal segmentation. We next segment the fused similarity matrix \mathbf{G} into contiguous task stages using Kernel Temporal Segmentation (KTS) [40], which partitions an ordered sequence into temporal segments rather than clustering frames independently, and controls segment count through a penalty without requiring an event classifier or pre-specified event types. KTS applies dynamic programming to identify boundaries that minimize within-segment variance:

$$\min_{L, \{b_j\}} \sum_{j=0}^{L-1} \left[\sum_{i=b_j}^{b_{j+1}-1} G_{ii} - \frac{1}{b_{j+1} - b_j} \sum_{i, i' \in [b_j, b_{j+1})} G_{ii'} \right] + \lambda L. \quad (1)$$

Since generative video backbones require fixed-length inputs, we expose K_{kf} as a user-configurable budget and bisection-search the penalty λ until KTS yields exactly that many intervals.

Explicit event coverage. KTS optimizes macroscopic stage boundaries, and we add a lightweight, optional post-processing step to explicitly protect short discrete events such as gripper transitions. When gripper commands are available, we detect sign changes $\mathcal{E}_g = \{t : \text{sign}(g_t) \neq \text{sign}(g_{t-1})\}$ and enforce coverage by replacing the nearest non-event candidate keyframe with the missed event frame. This post-processing preserves $|\mathcal{K}| = K_{\text{kf}}$, requires no event classifier or extra annotation, and directly protects the events that matter for policy learning.

Sparse keyframe generation. SKIP-SELECTOR runs only at training time, where it selects the indices \mathcal{K} from the dense ground-truth trajectory and turns the ordered sparse sequence $\mathcal{I}_{\mathcal{K}} = \{I_k : k \in \mathcal{K}\}$ into the supervision target. We fine-tune Wan 2.2-TI2V-5B [11] on this target conditioned only on the initial observation I_0 and language instruction c , giving the objective $\min_{\theta} \mathbb{E}_{\tau} [\mathcal{L}_{\text{Wan}}(\theta; I_0, c, \mathcal{I}_{\mathcal{K}})]$. At inference the dense trajectory is unavailable and SKIP-SELECTOR does not run, so the fine-tuned SKIP-GENERATOR instead produces the ordered K_{kf} keyframes $\hat{\mathcal{I}}_{\mathcal{K}}$ directly from (I_0, c) . SKIP-GENERATOR is thus action-free: the future actions \mathcal{A} enter only at the SKIP-RECONSTRUCTOR stage (§3.3), and keyframe-action consistency holds because in our offline data-augmentation setting the learned keyframes and the paired actions come from the same expert trajectories.

3.3 SKIP-RECONSTRUCTOR: Gap prediction and action-conditioned recovery

Using the sparse generated keyframes, we reconstruct a dense action-paired rollout in two steps. We first predict the number of intermediate frames in each inter-keyframe segment with a gap predictor, then fill them in with an action-conditioned flow interpolator, namely AC-FILM, guided by the corresponding action subsequence.

Gap prediction. For a selected keyframe sequence $\mathcal{K} = \{k_i\}_{i=0}^{K_{\text{kf}}-1}$, the ground-truth gap for segment i is $g_i = k_{i+1} - k_i$. During training, we encode adjacent target keyframes with a frozen image encoder and regress g_i from the concatenated features $[\mathbf{e}_i, \mathbf{e}_{i+1}, \mathbf{e}_{i+1} - \mathbf{e}_i]$. At synthesis time, we apply the same predictor to adjacent generated keyframes, then normalize the predicted lengths and convert them to integers so that $\sum_i \hat{g}_i = T - 1$, which preserves the original rollout length and decouples SKIP-GENERATOR from absolute timing.

Action-conditioned interpolation. Each inter-keyframe segment covers a short temporal interval, and the corresponding action subsequence specifies the underlying motion. Under this setting, a flow-based interpolator with low per-frame compute is sufficient as the backbone. We adopt FILM [41] for its stability under the large endpoint displacement between sparse keyframes. AC-FILM retains its recursive midpoint protocol, which subdivides each segment until reaching the target length. For segment i , we select the action sub-sequence \mathbf{A}_i of length \hat{g}_i and map it to a context vector \mathbf{z}_i with a lightweight 1D encoder using midpoint-query attention. We then use per-level FiLM projections [42] to convert \mathbf{z}_i into modulation parameters γ_{ℓ} and β_{ℓ} that scale and shift each pyramid level as $\mathbf{F}'_{\ell} = \gamma_{\ell} \odot \mathbf{F}_{\ell} + \beta_{\ell}$. To suppress modulation when the robot is nearly static, we gate the modulation through a convex blend $\mathbf{F}''_{\ell} = s \mathbf{F}'_{\ell} + (1 - s) \mathbf{F}_{\ell}$, where the action-magnitude score $s = \sigma(w_s \bar{m} + b_s)$ is derived from the mean pose-increment norm \bar{m} . As a result, the module is conservative on low-action intervals and action-aware around contact-rich motion. At inference, we apply AC-FILM recursively within each predicted gap to produce the dense action-paired rollout.

4 Experiments

We organize our experiments around three questions. **(i) Sparse-to-dense generation.** Does the proposed paradigm improve efficiency and generation quality over dense-generation and keyframe-selection baselines? **(ii) Replacing real demonstrations.** Can the generated videos match all-real policy training, and do they outperform dense-generated mixtures at the same mix ratio? **(iii) Ablation studies.** How does each component in SKIP affect performance?

4.1 Experimental setup

Benchmarks. We evaluate SKIP on the LIBERO simulation benchmark [18] and on a four-task Franka Panda real-robot platform with teleoperated demonstrations. On LIBERO we train SKIP-GENERATOR and SKIP-RECONSTRUCTOR on the SKIP-SELECTOR keyframes extracted from LIBERO-90, and evaluate on the four held-out suites.

Baselines and conditions. We compare against three categories of baselines, namely Uniform, RDP [43], and TriPSS [44] for keyframe selection, Wan 2.2-TI2V-5B [11] for fully dense video

generation, and action-free FILM [41] for interpolation. The five $\pi_{0.5}$ [6] policy training conditions share identical hyperparameters and differ only in data composition. Real uses all real demonstrations, SKIP-Mix70 and SKIP-Mix100 use 70% and 100% SKIP-generated videos with the remainder real, and Dense-Mix70 and Dense-Mix100 replace the synthetic portion with dense Wan 2.2 rollouts at the same ratios. We defer detailed preprocessing, splits, hyperparameters, hardware, and rollout protocols to Appendix A.

Evaluation Metrics. Since SKIP-SELECTOR is unsupervised, supervised keyframe metrics such as F1 do not apply [45]. We instead measure keyframe quality along two axes that are also robust to the uniform-sampling bias of linear-interpolation reconstruction, namely *event coverage* via GripCov and MEC, and *semantic span* via MaxSemDist and P95SemDist, summarized by a single operation-aware score $OAS = \frac{1}{4}[\text{GripCov} + \text{MEC} + (1 - \text{MaxSemDist}) + (1 - \text{P95SemDist})] \in [0, 1]$. Generated videos are evaluated using PSNR, SSIM [46], LPIPS [47], and FVD [48]. Downstream utility is measured by $\pi_{0.5}$ closed-loop success rate. We provide exact metric definitions in Appendix A, and verify that OAS tracks downstream success rate in Fig. 10 of Appendix C.

4.2 Sparse-to-dense generation

We evaluate the sparse-to-dense pipeline along three dimensions, namely the quality of the selected keyframes, the quality and cost of the reconstructed dense rollout, and the sensitivity to the keyframe budget K_{kf} .

Selection quality. We first evaluate whether SKIP-SELECTOR captures the structural state changes that baselines often miss. Uniform and RDP test geometric selection without an event-aware mechanism, while TriPSS tests visual clustering without temporal order.

As shown in Tab. 1, SKIP-SELECTOR leads on every metric, with the largest margin on GripCov and a +0.063 OAS gap. We attribute this to the combination of multimodal fusion and explicit gripper-event protection, which jointly preserve the critical manipulation events. Per-event-count breakdowns (Fig. 5), event-hit visualizations (Fig. 6), and per-stream ablations (Tab. 19(a)) are in Appendix C.

Generated video quality. We then evaluate the pixel-level and feature-level quality of the dense rollout. The keyframe-selector baselines share the same flow interpolator with SKIP, while Wan 2.2 replaces the entire pipeline with chunked dense generation.

As shown in Tab. 2, SKIP leads on all metrics, and on every suite-metric cell in the per-suite breakdown (Tab. 10). The dense Wan 2.2 baseline produces FVD $3\times$ to $15\times$ higher than any sparse-anchor pipeline, indicating that sparse-to-dense generation avoids the long-horizon drift accumulated by chunked recursive sampling. Qualitative success and failure rollouts are in Fig. 9.

Efficiency. As shown in Tab. 3, SKIP achieves a $4.16\times$ average speedup over recursive dense Wan 2.2 generation. The cost is dominated by keyframe generation at ~ 35 s per trajectory, while gap prediction and interpolation together add only ~ 3 s.

Budget configurability. At the keyframe-extraction stage, K_{kf} can be set by the user or auto-selected per trajectory via the BIC criterion. Sweeping $K_{\text{kf}} \in \{9, 17, 33, 41, 57\}$ in Appendix C produces the cost-quality curve in Fig. 7, with an elbow at $K_{\text{kf}}=41$ matching the median BIC-selected count on LIBERO-90. We therefore fix $K_{\text{kf}}=41$ across the rest of the pipeline in this work, reflecting the data’s intrinsic event density rather than manual tuning.

Table 1: **Keyframe selection quality across the four LIBERO test suites at $K_{\text{kf}}=41$.**

Method	MEC \uparrow	GripCov \uparrow	MaxSemDist \downarrow	P95SemDist \downarrow	OAS \uparrow
Uniform	0.779	0.771	0.137	0.111	0.825
RDP	0.855	0.864	0.189	0.137	0.848
TriPSS	0.702	0.711	0.145	0.117	0.787
SKIP-Selector (Ours)	0.888	0.999	0.132	0.109	0.911

Table 2: **End-to-end video quality on LIBERO test suites (averaged across four suites):** Per-suite breakdown in Tab. 10 of Appendix C.1.

Method	PSNR \uparrow	SSIM \uparrow	LPIPS \downarrow	FVD \downarrow
Wan 2.2 (chunked)	21.423	0.832	0.162	4177
Uniform	21.345	0.847	0.130	716
RDP	21.076	0.843	0.137	724
TriPSS	21.033	0.827	0.157	640
SKIP (Ours)	21.635	0.856	0.119	458

Table 3: **End-to-end inference time on LIBERO:** We report seconds per trajectory on one H2O GPU, where both methods use 50 denoising steps and bf16 precision.

Suite	SKIP (Ours)				Wan 2.2 (chunked) \downarrow	Speedup \uparrow
	Keyframe gen.	Gap pred.	Interp.	Total \downarrow		
LIBERO-10	34.78	0.23	4.78	39.79	243.86	6.13\times
LIBERO-Goal	35.24	0.02	2.47	37.73	144.66	3.83\times
LIBERO-Object	35.45	0.02	2.28	37.75	137.92	3.65\times
LIBERO-Spatial	34.68	0.02	1.94	36.64	124.74	3.40\times
Weighted avg.	35.06	0.06	2.74	37.86	157.37	4.16\times

4.3 Replacing real demonstrations

Video metrics alone do not establish whether generated rollouts can serve as effective policy-training data. We therefore train $\pi_{0.5}$ policies with identical hyperparameters and vary only the data composition.

Matching all-real training. As shown in Fig. 3, SKIP-Mix70 matches all-real training within 1 pp on both platforms, costing 0.28 pp on LIBERO and 0.84 pp on the real robot. Even with all real data removed, SKIP-Mix100 drops only another ~ 1 pp in simulation, showing that SKIP videos alone can sustain near all-real policy performance.

Drift collapse on dense baselines. Against the matched Dense-Mix baselines, SKIP-Mix70 outperforms Dense-Mix70 by 29.9 pp in simulation and 32.5 pp on the real robot, and the gap widens to 56.4 and 41.7 pp at 100% synthetic. The drift accumulated by dense 49-frame stitching propagates into the policy, so it is high-fidelity sparse generation, not the mere presence of synthetic video, that enables SKIP rollouts to substitute for real demonstrations. Per-suite and per-task breakdowns are in Tab. 14 and Tab. 15.

4.4 Ablation studies

We ablate two design groups in SKIP, namely the keyframe-selection design in SKIP-SELECTOR and the action conditioning in SKIP-RECONSTRUCTOR. Each ablation uses the same downstream $\pi_{0.5}$ success-rate protocol as §4.3, with results in Tab. 4.

Keyframe selection. As shown in Tab. 4, no single stream suffices. Multimodal fusion progressively lifts performance, and gripper-event post-processing yields a further gain. The pattern suggests that smooth multimodal fusion captures the coarse manipulation structure, while explicit gripper-event protection safeguards the short discrete events that decide successful grasps. Per-stream selection-quality breakdowns are in Tab. 19(a).

Action conditioning. As shown in Tab. 4, AC-FILM improves both simulation and real-robot success over action-free FILM. The corresponding per-trajectory PSNR/SSIM/LPIPS improvements on dense recovery are reliable under a paired t -test at $p < 0.01$, with full breakdowns in Tab. 19(b). Action conditioning supplies the physical prior that matters around occlusions and contact transitions, where visual endpoints alone underconstrain robot motion. We further ablate the temporal segmentation choice against four alternatives (Uniform partition, Spectral clustering [49], Agglomerative clustering [50], Bayesian change-point [51]) in §C.1, and the fusion weighting against three strategies

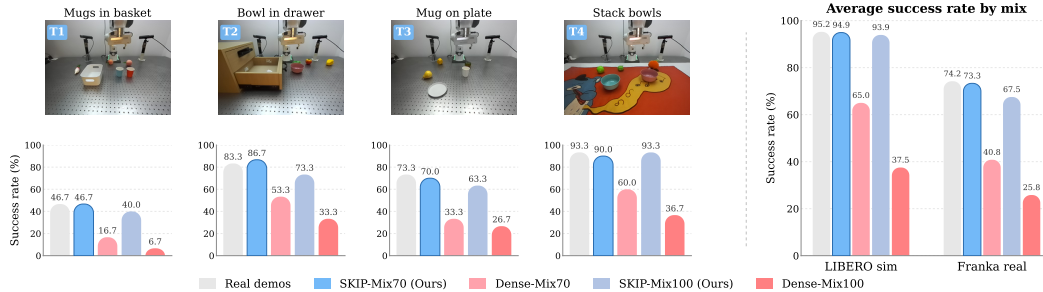


Figure 3: $\pi_{0.5}$ success rate across five training mixes. **Left:** screenshots of the four Franka Panda real-robot tasks T1 to T4 with their names labelled above, and per-task success rate over 30 rollouts shown as bar charts below each task. **Right:** average success rate on LIBERO simulation and on the Franka real robot.

Table 4: **Downstream $\pi_{0.5}$ ablations of SKIP design components:** Gripper is the gripper-event post-processing in SKIP-SELECTOR and Action is action conditioning in the interpolator.

Visual	Keyframe selection			Gripper	Recovery Action	Avg. SR (%) \uparrow	
	Semantic	Proprioceptive				Sim	Real
✓	✗	✗	✗	✗	✓	71.5	43.3
✗	✓	✗	✗	✗	✓	68.7	36.7
✗	✗	✓	✗	✗	✓	73.6	50.0
✓	✓	✗	✗	✗	✓	81.2	53.3
✓	✓	✓	✗	✗	✓	91.4	66.7
✓	✓	✓	✓	✓	✗	90.4	66.7
✓	✓	✓	✓	✓	✓	94.9	73.3

(effective-rank-weighted, fixed-weight, grid search) in §C.3. Both confirm KTS and equal weighting as the strongest configurations on every metric reported.

5 Conclusion

We propose SKIP, a sparse keyframe interpolation framework for embodied world models that selects event-preserving keyframes through robot-aware multimodal fusion, generates only those keyframes with a video diffusion model, and reconstructs dense action-aligned rollouts via a learned gap predictor and an action-conditioned interpolator. On the LIBERO benchmark and a four-task Franka Panda real-robot platform, SKIP produces dense rollouts $4.16\times$ faster than a dense Wan 2.2 baseline while reducing aggregate FVD by 89.0%, and SKIP videos are effective policy-training data. Even fully replacing real demonstrations drops $\pi_{0.5}$ success by only 1.3 pp in simulation and 6.7 pp on the real robot, whereas fully dense-generated rollouts collapse by 48 to 58 pp. These results suggest that, on the manipulation benchmarks studied, much of a dense rollout can be recovered from a few decisive manipulation events, opening a practical path toward scalable visual data for robot policy learning and applications such as planning preview and behavior-level inspection.

6 Limitations

Our method assumes a fixed third-person camera and a single-arm manipulator, and has been evaluated on a limited set of datasets. Its clearest failure mode is on long compound episodes, where errors near phase switches accumulate in the dense reconstruction, which explicit phase-aware recovery could address. We plan to extend our approach in three directions. First, we will evaluate on more datasets and policy backbones to test general effectiveness. Second, we will adapt the event-driven keyframe strategy to multi-view and bimanual manipulation. Third, we will train vision-language-action models on keyframes alone rather than dense video, testing whether sparse event-aware training preserves policy performance at lower compute.

References

- [1] A. Brohan, N. Brown, J. Carbajal, Y. Chebotar, J. Dabis, C. Finn, K. Gopalakrishnan, K. Hausman, A. Herzog, J. Hsu, et al. Rt-1: Robotics transformer for real-world control at scale. *Robotics: Science and Systems XIX*, 2023.
- [2] B. Zitkovich, T. Yu, S. Xu, P. Xu, T. Xiao, F. Xia, J. Wu, P. Wohlhart, S. Welker, A. Wahid, et al. Rt-2: Vision-language-action models transfer web knowledge to robotic control. In *Conference on Robot Learning*, pages 2165–2183. PMLR, 2023.
- [3] M. J. Kim, K. Pertsch, S. Karamcheti, T. Xiao, A. Balakrishna, S. Nair, R. Rafailov, E. P. Foster, P. R. Sanketi, Q. Vuong, et al. Openvla: An open-source vision-language-action model. In *Conference on Robot Learning*, pages 2679–2713. PMLR, 2025.
- [4] O. M. Team, D. Ghosh, H. Walke, K. Pertsch, K. Black, O. Mees, S. Dasari, J. Hejna, T. Kreiman, C. Xu, et al. Octo: An open-source generalist robot policy. *arXiv preprint arXiv:2405.12213*, 2024.
- [5] K. Black, N. Brown, D. Driess, A. Esmail, M. Equi, C. Finn, N. Fusai, L. Groom, K. Hausman, B. Ichter, et al. π_0 : A vision-language-action flow model for general robot control. *arXiv preprint arXiv:2410.24164*, 2024.
- [6] K. Black, N. Brown, J. Darpinian, K. Dhabalia, D. Driess, A. Esmail, M. R. Equi, C. Finn, N. Fusai, M. Y. Galliker, et al. $\pi_{0.5}$: a vision-language-action model with open-world generalization. In *9th Annual Conference on Robot Learning*, 2025.
- [7] P. Li, Y. Chen, H. Wu, X. Ma, X. Wu, Y. Huang, L. Wang, T. Kong, and T. Tan. Bridgevla: Input-output alignment for efficient 3d manipulation learning with vision-language models. *Advances in Neural Information Processing Systems*, 38:63635–63673, 2026.
- [8] W. Peebles and S. Xie. Scalable diffusion models with transformers. In *Proceedings of the IEEE/CVF international conference on computer vision*, pages 4195–4205, 2023.
- [9] T. Brooks, B. Peebles, C. Holmes, W. DePue, Y. Guo, L. Jing, D. Schnurr, J. Taylor, T. Luhman, E. Luhman, C. Ng, R. Wang, and A. Ramesh. Video generation models as world simulators. 2024. URL <https://openai.com/research/video-generation-models-as-world-simulators>.
- [10] Z. Yang, J. Teng, W. Zheng, M. Ding, S. Huang, J. Xu, Y. Yang, W. Hong, X. Zhang, G. Feng, et al. Cogvideox: Text-to-video diffusion models with an expert transformer. In *International Conference on Learning Representations*, volume 2025, pages 83048–83077, 2025.
- [11] T. Wan, A. Wang, B. Ai, B. Wen, C. Mao, C.-W. Xie, D. Chen, F. Yu, H. Zhao, J. Yang, et al. Wan: Open and advanced large-scale video generative models. *arXiv preprint arXiv:2503.20314*, 2025.
- [12] M. Gygli, H. Grabner, H. Riemenschneider, and L. Van Gool. Creating summaries from user videos. In *European conference on computer vision*, pages 505–520. Springer, 2014.
- [13] K. Zhou, Y. Qiao, and T. Xiang. Deep reinforcement learning for unsupervised video summarization with diversity-representativeness reward. In *Proceedings of the AAAI conference on artificial intelligence*, volume 32, 2018.
- [14] T. Lin, X. Liu, X. Li, E. Ding, and S. Wen. Bmn: Boundary-matching network for temporal action proposal generation. In *Proceedings of the IEEE/CVF international conference on computer vision*, pages 3889–3898, 2019.
- [15] C.-L. Zhang, J. Wu, and Y. Li. Actionformer: Localizing moments of actions with transformers. In *European Conference on Computer Vision*, pages 492–510. Springer, 2022.

- [16] C. Zhao, M. Liu, W. Wang, W. Chen, F. Wang, H. Chen, B. Zhang, and C. Shen. Moviedreamer: Hierarchical generation for coherent long visual sequences. In *International Conference on Learning Representations*, volume 2025, pages 50060–50090, 2025.
- [17] X. Wang, J. Liu, Z. Wang, X. Yu, J. Wu, X. Sun, Y. Su, A. Yuille, Z. Liu, and E. Barsoum. Keyvid: Keyframe-aware video diffusion for audio-synchronized visual animation. *arXiv preprint arXiv:2504.09656*, 2025.
- [18] B. Liu, Y. Zhu, C. Gao, Y. Feng, Q. Liu, Y. Zhu, and P. Stone. Libero: Benchmarking knowledge transfer for lifelong robot learning. *Advances in Neural Information Processing Systems*, 36: 44776–44791, 2023.
- [19] D. Hafner, T. Lillicrap, J. Ba, and M. Norouzi. Dream to control: Learning behaviors by latent imagination. In *International Conference on Learning Representations*, 2020. URL <https://openreview.net/forum?id=S110TC4tDS>.
- [20] D. Hafner, J. Pasukonis, J. Ba, and T. Lillicrap. Mastering diverse control tasks through world models. *Nature*, 640(8059):647–653, 2025.
- [21] N. Hansen, H. Su, and X. Wang. Td-mpc2: Scalable, robust world models for continuous control. In *International Conference on Learning Representations*, volume 2024, pages 47376–47405, 2024.
- [22] A. Bardes, Q. Garrido, J. Ponce, X. Chen, M. Rabbat, Y. LeCun, M. Assran, and N. Ballas. Revisiting feature prediction for learning visual representations from video. *Transactions on Machine Learning Research*, 2024. ISSN 2835-8856. URL <https://openreview.net/forum?id=QaCCuDfBk2>. Featured Certification.
- [23] M. Assran, A. Bardes, D. Fan, Q. Garrido, R. Howes, M. Muckley, A. Rizvi, C. Roberts, K. Sinha, A. Zholus, et al. V-jepa 2: Self-supervised video models enable understanding, prediction and planning. *arXiv preprint arXiv:2506.09985*, 2025.
- [24] F. Zhu, H. Wu, S. Guo, Y. Liu, C. Cheang, and T. Kong. Irasim: A fine-grained world model for robot manipulation. In *Proceedings of the IEEE/CVF International Conference on Computer Vision*, pages 9834–9844, 2025.
- [25] A. Mandlekar, S. Nasiriany, B. Wen, I. Akinola, Y. Narang, L. Fan, Y. Zhu, and D. Fox. Mimicgen: A data generation system for scalable robot learning using human demonstrations. In *Conference on Robot Learning*, pages 1820–1864. PMLR, 2023.
- [26] Z. Chen, S. Kiami, A. Gupta, and V. Kumar. Genaug: Retargeting behaviors to unseen situations via generative augmentation. *arXiv preprint arXiv:2302.06671*, 2023.
- [27] Y. Wang, Z. Xian, F. Chen, T.-H. Wang, Y. Wang, K. Fragkiadaki, Z. Erickson, D. Held, and C. Gan. Robogen: towards unleashing infinite data for automated robot learning via generative simulation. In *Proceedings of the 41st International Conference on Machine Learning*, pages 51936–51983, 2024.
- [28] J. Bae, I. Hwang, Y.-Y. Lee, Z. Guo, J. Liu, Y. Ben-Shabat, Y. M. Kim, and M. Kapadia. Less is more: Improving motion diffusion models with sparse keyframes. In *Proceedings of the IEEE/CVF International Conference on Computer Vision*, pages 11069–11078, 2025.
- [29] S. Li, Q. Hao, Y. Shang, and Y. Li. Keyworld: Key frame reasoning enables effective and efficient world models. *arXiv preprint arXiv:2509.21027*, 2025.
- [30] L. Yang, Y. Bai, G. Eskandar, F. Shen, M. Altillawi, D. Chen, S. Majumder, Z. Liu, G. Kutyniok, and A. Valada. Roboenvision: A long-horizon video generation model for multi-task robot manipulation. In *2025 IEEE/RSJ International Conference on Intelligent Robots and Systems (IROS)*, pages 21281–21288. IEEE, 2025.

- [31] H. Jiang, D. Sun, V. Jampani, M.-H. Yang, E. Learned-Miller, and J. Kautz. Super slomo: High quality estimation of multiple intermediate frames for video interpolation. In *Proceedings of the IEEE conference on computer vision and pattern recognition*, pages 9000–9008, 2018.
- [32] Z. Huang, T. Zhang, W. Heng, B. Shi, and S. Zhou. Real-time intermediate flow estimation for video frame interpolation. In *European conference on computer vision*, pages 624–642. Springer, 2022.
- [33] Z. Li, Z.-L. Zhu, L.-H. Han, Q. Hou, C.-L. Guo, and M.-M. Cheng. Amt: All-pairs multi-field transforms for efficient frame interpolation. In *Proceedings of the IEEE/CVF Conference on Computer Vision and Pattern Recognition*, pages 9801–9810, 2023.
- [34] J. Oh, X. Guo, H. Lee, R. L. Lewis, and S. Singh. Action-conditional video prediction using deep networks in atari games. *Advances in neural information processing systems*, 28, 2015.
- [35] C. Finn and S. Levine. Deep visual foresight for planning robot motion. In *2017 IEEE international conference on robotics and automation (ICRA)*, pages 2786–2793. IEEE, 2017.
- [36] F. Ebert, C. Finn, S. Dasari, A. Xie, A. Lee, and S. Levine. Visual foresight: Model-based deep reinforcement learning for vision-based robotic control. *arXiv preprint arXiv:1812.00568*, 2018.
- [37] O. Siméoni, H. V. Vo, M. Seitzer, F. Baldassarre, M. Oquab, C. Jose, V. Khalidov, M. Szafraniec, S. Yi, M. Ramamonjisoa, et al. Dinov3. *arXiv preprint arXiv:2508.10104*, 2025.
- [38] M. Oquab, T. Darcet, T. Moutakanni, H. Vo, M. Szafraniec, V. Khalidov, P. Fernandez, D. Haziza, F. Massa, A. El-Nouby, et al. Dinov2: Learning robust visual features without supervision. *Transactions on Machine Learning Research Journal*, 2024.
- [39] B. Schölkopf, A. Smola, and A. F. Atiya. Learning with kernels: Support vector machines, regularization, optimization, and beyond. *IEEE Transactions on Information Theory*, 16(3): 781–781, 2005.
- [40] D. Potapov, M. Douze, Z. Harchaoui, and C. Schmid. Category-specific video summarization. In *European conference on computer vision*, pages 540–555. Springer, 2014.
- [41] F. Reda, J. Kontkanen, E. Tabellion, D. Sun, C. Pantofaru, and B. Curless. Film: Frame interpolation for large motion. In *European Conference on Computer Vision*, pages 250–266. Springer, 2022.
- [42] E. Perez, F. Strub, H. De Vries, V. Dumoulin, and A. Courville. Film: Visual reasoning with a general conditioning layer. In *Proceedings of the AAAI conference on artificial intelligence*, volume 32, 2018.
- [43] D. H. Douglas and T. K. Peucker. Algorithms for the reduction of the number of points required to represent a digitized line or its caricature. *Cartographica: the international journal for geographic information and geovisualization*, 10(2):112–122, 1973.
- [44] M. C. Cakmak, N. Agarwal, and D. Poudel. Tripss: A tri-modal keyframe extraction framework using perceptual, structural, and semantic representations. *arXiv preprint arXiv:2506.05395*, 2025.
- [45] M. Otani, Y. Nakashima, E. Rahtu, and J. Heikkila. Rethinking the evaluation of video summaries. In *Proceedings of the IEEE/CVF conference on computer vision and pattern recognition*, pages 7596–7604, 2019.
- [46] Z. Wang, A. C. Bovik, H. R. Sheikh, and E. P. Simoncelli. Image quality assessment: from error visibility to structural similarity. *IEEE transactions on image processing*, 13(4):600–612, 2004.

- [47] R. Zhang, P. Isola, A. A. Efros, E. Shechtman, and O. Wang. The unreasonable effectiveness of deep features as a perceptual metric. In *Proceedings of the IEEE conference on computer vision and pattern recognition*, pages 586–595, 2018.
- [48] T. Unterthiner, S. Van Steenkiste, K. Kurach, R. Marinier, M. Michalski, and S. Gelly. Towards accurate generative models of video: A new metric & challenges. *arXiv preprint arXiv:1812.01717*, 2018.
- [49] A. Ng, M. Jordan, and Y. Weiss. On spectral clustering: Analysis and an algorithm. *Advances in neural information processing systems*, 14, 2001.
- [50] J. H. Ward Jr. Hierarchical grouping to optimize an objective function. *Journal of the American statistical association*, 58(301):236–244, 1963.
- [51] R. P. Adams and D. J. MacKay. Bayesian online changepoint detection. *arXiv preprint arXiv:0710.3742*, 2007.
- [52] K. He, X. Zhang, S. Ren, and J. Sun. Deep residual learning for image recognition. In *Proceedings of the IEEE conference on computer vision and pattern recognition*, pages 770–778, 2016.
- [53] H. Xu, J. Zhang, J. Cai, H. Rezatofghi, F. Yu, D. Tao, and A. Geiger. Unifying flow, stereo and depth estimation. *IEEE Transactions on Pattern Analysis and Machine Intelligence*, 45(11): 13941–13958, 2023.
- [54] H. Wang, A. Kläser, C. Schmid, and C.-L. Liu. Dense trajectories and motion boundary descriptors for action recognition. *International journal of computer vision*, 103(1):60–79, 2013.

Appendix overview. Appendix A details the datasets, splits, baselines, and evaluation metrics. Appendix B reports hardware, training hyperparameters, and feature-stream specifications. Appendix C provides supplementary diagnostics extending the main experiments, organized into three subsections that follow the main paper’s experimental flow, namely sparse-to-dense generation (§4.2), policy-data results (§4.3), and ablation studies (§4.4).

A Datasets and evaluation protocol

Tab. 5 lists the source datasets and trajectory counts, and Fig. 4 visualizes the four real-robot tasks.

Table 5: **Datasets at a glance.** All LIBERO numbers are no-op-filtered trajectory counts. The four real-robot tasks total 192 demonstrations.

Dataset	Source	# Trajectories
libero_90	LIBERO	3528
libero_10	LIBERO	301
libero_goal	LIBERO	376
libero_object	LIBERO	432
libero_spatial	LIBERO	394
T1: put both the red mug and the blue mug in the basket	Franka Panda teleop	48
T2: put the red bowl in the drawer and close the drawer	Franka Panda teleop	48
T3: put the white mug on the plate	Franka Panda teleop	48
T4: stack the red bowl on the green bowl	Franka Panda teleop	48

A.1 LIBERO simulation

LIBERO contains five suites totalling 5031 trajectories after no-op filtering. Raw episodes are unified into a trajectory format with RGB frames, actions, proprioception, and language instructions following [29], and the no-op-filtered version (semantically equivalent to the official `*_no_noops` RLDS preprocessing) is used after discarding dummy episodes. RGB frames are bicubic-resized from 512×512 to 256×256 , and $\pi_{0.5}$ further pads them to 224×224 for the PaliGemma encoder. The raw 9-D LIBERO state (gripper $\times 2$, end-effector position, quaternion) is converted to an 8-D vector via axis-angle representation, and actions remain 7-D continuous commands.

Splits. `libero_90` (3528 traj) is the training pool for the full SKIP pipeline, namely SKIP-Selector keyframe extraction, SKIP-Generator fine-tuning, and SKIP-Reconstructor training all run on `libero_90`. The other four suites (`libero_10` / `goal` / `object` / `spatial`, 1503 traj) are held out for SKIP video-quality evaluation, reported in Tab. 1 through Tab. 3. The same four suites also serve as the source for downstream $\pi_{0.5}$ studies, providing the 1503 trajectories on which the five training conditions defined in §4.1 (Real demos, SKIP-Mix70/100, Dense-Mix70/100) are built. Each policy is evaluated via closed-loop rollouts on the same four suites.

A.2 Real-robot platform

The platform is a 7-DoF Franka Emika Panda with a single third-person RGB camera. Fig. 4 shows the four manipulation tasks, namely sequential pick-and-place (T1), pick-and-place plus drawer operation (T2), single pick-and-place (T3), and object stacking (T4). We collect 48 teleoperated demonstrations per task, totalling 192 episodes. $\pi_{0.5}$ training uses the same five conditions as in simulation (Real demos, SKIP-Mix70/100, Dense-Mix70/100), with the SKIP synthetic portion produced by a SKIP pipeline separately fine-tuned on real-robot demonstrations. Evaluation is 30 closed-loop rollouts per task with initial placements randomized within a fixed range.

A.3 Baselines and metrics

Keyframe baselines all use the same budget $K_{kf}=41$. Uniform selects equispaced frames, RDP [43] follows the KeyWorld [29] choice, and TriPSS [44] applies HDBSCAN over three visual streams. The **dense video baseline** is Wan 2.2-TI2V-5B [11] fine-tuned on dense 49-frame chunks of LIBERO-90

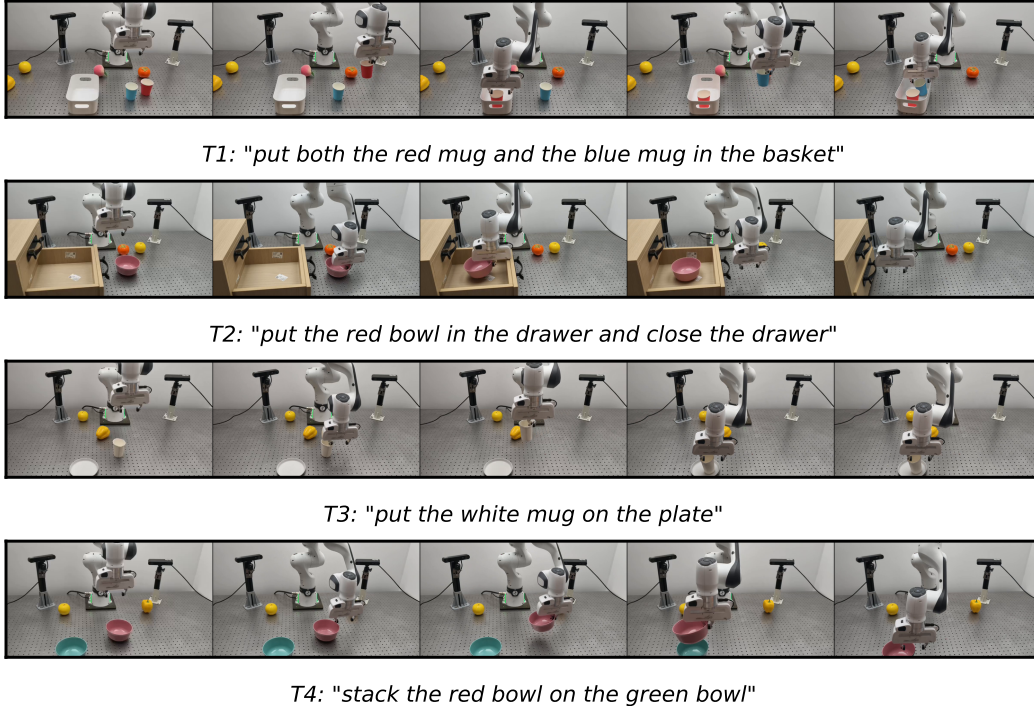


Figure 4: **Real-robot task overview.** Each row corresponds to one task and matches the T1–T4 columns of Tab. 15.

with the same recipe and training pool as SKIP-GENERATOR, run recursively chunk by chunk at synthesis time. This matches SKIP’s training data and protocol, isolating the effect of sparse versus dense generation from any data-exposure or training-recipe asymmetry. The **interpolation baseline** is action-free FILM [41] fine-tuned on the same SKIP-Selector keyframes with the same recipe as AC-FILM.

Keyframe-quality metrics. We avoid supervised metrics such as F1, which are known to be sensitive to video pre-segmentation rather than to the keyframe algorithm itself [45], and instead use unsupervised coverage measures. GripCov is the fraction of gripper sign-change events covered within ± 2 frames. MEC applies the same ± 2 -frame coverage to four event types (gripper sign change, joint-velocity spike, trajectory turning point, acceleration burst). MaxSemDist is the maximum cosine distance between adjacent keyframes’ DINOv3 features and P95SemDist its 95th percentile. **Video quality** uses PSNR, SSIM, and LPIPS at 256×256 , plus FVD via an I3D backbone. **Downstream utility** is measured by $\pi_{0.5}$ closed-loop success rate.

B Implementation Details

B.1 Training and inference configuration

Table 6 lists every training and inference configuration for reproducibility, including the System, SKIP-GENERATOR, Gap predictor, AC-FILM, and $\pi_{0.5}$ fine-tune blocks.

B.2 Multimodal feature streams

The three feature streams that feed SKIP-SELECTOR are described below. All streams are computed offline on the full dataset and cached before SKIP-SELECTOR runs.

Visual stream (V). We compute UniMatch [53] optical flow between consecutive frames, then summarize each flow field with a histogram-of-flow (HoF) descriptor following Wang et al. [54]:

Table 6: **Implementation details.**

Module	Element	Detail
System	OS	Ubuntu 22.04
	CUDA	12.1
	Python	3.10
	PyTorch	2.4.1
	Device	8 × NVIDIA H20
SKIP-GENERATOR	Batch size	1
	Epochs	30
	Resolution	256 × 256
	Optimizer	AdamW
	Learning rate	1e-5
	Precision	bf16
	Trainable modules	DiT only (VAE/text-encoder frozen)
Gap predictor	Encoder	frozen ResNet-50 [52]
	Batch size	8
	Epochs	100
	Optimizer	Adam
	Learning rate	3e-4
AC-FILM	Batch size	4
	Epochs	20 (1 backbone-frozen + 19 joint)
	Optimizer	AdamW
	Learning rate	2e-4
	Weight decay	1e-5
	Loss	ℓ_1 + VGG perceptual + Gram style
	FiLM proj. init	Zero (identity at start)
$\pi_{0.5}$ fine-tune	Batch size	32
	Steps	30 000
	Optimizer	AdamW (cosine schedule)
	Learning rate	5e-5 (peak)
	Precision	bf16 + gradient checkpointing

a 2×2 spatial grid, 8 orientation bins, and a low-magnitude (‘zero-flow’) bin, yielding $4 \times 9 = 36$ dimensions. The last frame’s descriptor is duplicated to align with the image count.

Semantic stream (S). DINOv3 ViT-L/16 [37] features are extracted at 224×224 with ImageNet normalization. We concatenate the CLS token and the mean of the patch tokens, producing a 2048-D vector, and L2-normalize.

Proprioceptive stream (P). Six feature groups, 41 dimensions in total: raw state (8), first-order velocity (8), second-order acceleration (8), multi-scale RDP perpendicular distances at window radii $\{3, 5, 9, 15, 25\}$ in both the position subspace and the full state ($5 \times 2 = 10$), multi-scale Menger curvatures of the position trajectory (5), and gripper change rate plus binary open/close event (2). All states are first converted to axis-angle for rotation, with a sequential unwrapping step to handle the $\theta_r = \pi$ discontinuity of quaternion-to-axis-angle conversion. Each group is z-score normalized before concatenation.

C Supplementary diagnostics

This section extends the main experiments of §4 in order. We first add analyses of the sparse-to-dense generation experiments from §4.2, then breakdowns of the policy-data experiments from §4.3, and finally intermediate-metric ablations for §4.4.

C.1 Sparse-to-dense generation extensions (§4.2)

Selection-quality details. Per-event-count keyframe-quality breakdown. As shown in Fig. 5, binning held-out LIBERO trajectories by gripper-event count per episode reveals that SKIP-SELECTOR’s GripCov stays above 0.99 on every bin including the 5+-event bin, while Uniform’s GripCov drops sharply. The margin over Uniform, RDP, and TriPSS widens monotonically with manipulation complexity.

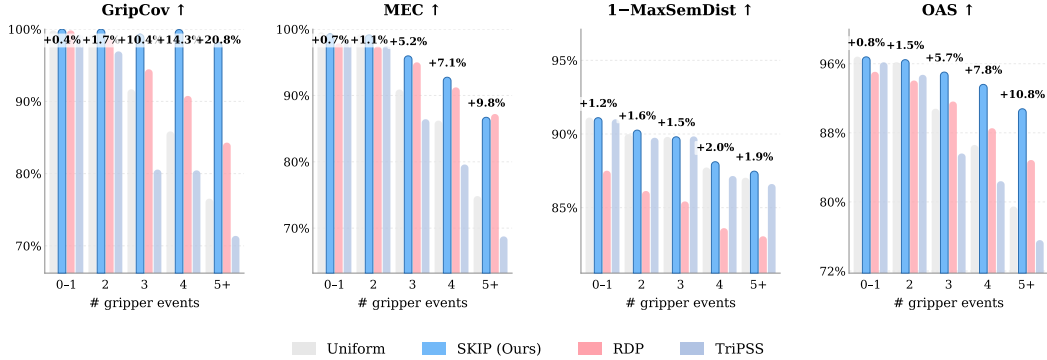


Figure 5: **Per-event-count keyframe-quality breakdown.** Held-out LIBERO trajectories are bucketed by gripper-event count (0–1, 2, 3, 4, 5+), with each panel reporting a different keyframe-quality metric. SKIP-SELECTOR’s margin over Uniform, RDP, and TriPSS widens as manipulation complexity grows, with the largest gains on the 5+-event bucket.

Per-trajectory event-hit visualization. As shown in Fig. 6, on a representative LIBERO trajectory with four ground-truth gripper events, SKIP-SELECTOR hits all four exactly while Uniform, RDP, and TriPSS each miss multiple events.

Per-suite selection-quality breakdown. While main-body Tab. 1 reports only across-suite averages, the per-suite breakdown in Tab. 7 exposes whether SKIP-SELECTOR’s average advantage is uniform across LIBERO suites or driven by specific ones. SKIP-SELECTOR strictly outperforms every baseline on every (suite, metric) cell, because the multimodal fusion combines event-coverage signals (MEC, GripCov) with semantic-span signals (MaxSemDist, P95SemDist) that no single-modality baseline can match across the diverse task distributions of LIBERO. The AVG block at the bottom matches Tab. 1.

Table 7: **Per-suite selection-quality breakdown.** AVG block at bottom matches Tab. 1.

Suite	Method	MEC↑	GripCov↑	MaxSemDist↓	P95SemDist↓	OAS↑
LIBERO-10	Uniform	0.755	0.748	0.157	0.125	0.805
	RDP	0.838	0.846	0.213	0.150	0.830
	TriPSS	0.685	0.694	0.160	0.128	0.773
	SKIP-Selector (Ours)	0.872	0.997	0.152	0.123	0.899
LIBERO-Goal	Uniform	0.788	0.781	0.135	0.110	0.831
	RDP	0.860	0.870	0.184	0.135	0.853
	TriPSS	0.706	0.714	0.142	0.114	0.791
	SKIP-Selector (Ours)	0.890	0.999	0.128	0.108	0.913
LIBERO-Object	Uniform	0.770	0.760	0.147	0.115	0.817
	RDP	0.847	0.857	0.198	0.142	0.841
	TriPSS	0.694	0.702	0.155	0.118	0.781
	SKIP-Selector (Ours)	0.880	0.999	0.141	0.113	0.906
LIBERO-Spatial	Uniform	0.799	0.791	0.113	0.098	0.845
	RDP	0.871	0.879	0.165	0.125	0.865
	TriPSS	0.719	0.730	0.127	0.112	0.802
	SKIP-Selector (Ours)	0.906	0.999	0.111	0.096	0.924
AVG	Uniform	0.779	0.771	0.137	0.111	0.825
	RDP	0.855	0.864	0.189	0.137	0.848
	TriPSS	0.702	0.711	0.145	0.117	0.787
	SKIP-Selector (Ours)	0.888	0.999	0.132	0.109	0.911

Segmenter selection quality. To isolate the contribution of KTS dynamic programming, we replace the temporal segmentation step with four alternatives while holding V/S/P fusion and gripper-event post-processing fixed. The alternatives span uniform partitioning (which ignores the affinity matrix), spectral clustering [49] (k -cut without temporal-order constraints), agglomerative clustering [50] (local similarity), and Bayesian online change-point detection [51] (explicit temporal segments). As shown in Tab. 8, KTS leads on every selection-quality metric. The largest GripCov margin (KTS



Figure 6: **Per-trajectory event-hit visualization of keyframe selection.** A LIBERO trajectory with four ground-truth gripper events. For each method, the column shows the chosen keyframe closest to each event with its frame offset and any missed event. SKIP-SELECTOR (bottom row) hits all four events exactly, while Uniform, RDP, and TriPSS each miss multiple events.

0.999 vs. Bayesian change-point 0.972, a 0.027 gap) reflects the dynamic-programming objective’s ability to land boundaries precisely on event transitions rather than near them. Bayesian online change-point is the closest competitor on OAS (0.891 vs. KTS 0.911) because it also leverages temporal order, but its locally-greedy segmentation does not optimize the global within-segment variance KTS minimizes. The three no-temporal-order baselines (Uniform / Spectral / Agglomerative) trail by between 0.033 and 0.096 OAS.

Table 8: **Alternative temporal segmenters: selection quality.**

Segmenter	MEC \uparrow	GripCov \uparrow	MaxSemDist \downarrow	P95SemDist \downarrow	OAS \uparrow
Uniform partition on \mathbf{G}	0.748	0.815	0.162	0.142	0.815
Spectral clustering (k -cut)	0.838	0.875	0.155	0.130	0.857
Agglomerative clustering	0.832	0.952	0.149	0.124	0.878
Bayesian online change-point	0.846	0.972	0.139	0.116	0.891
KTS (Ours)	0.888	0.999	0.132	0.109	0.911

Segmenter downstream SR. As shown in Tab. 9, the SR ranking follows the selection-quality ranking of Tab. 8, namely KTS > Bayesian change-point > Agglomerative > Spectral > Uniform on both LIBERO sim avg and Franka real avg. KTS-Mix100 reaches 93.9% sim and 67.5% real, beating the second-best Bayesian change-point by 5.9 pp sim and 7.5 pp real. The two no-temporal-order baselines (Uniform partition on \mathbf{G} and Spectral clustering) trail by between 11.5 and 17.7 pp on sim

and between 11.7 and 18.3 pp on real, confirming that explicit temporal segmentation is essential for downstream policy performance.

Table 9: **Alternative temporal segmenters: downstream $\pi_{0.5}$ SR (Mix100)**. Each alternative pipes its keyframes through identical SKIP-Generator + SKIP-Reconstructor + $\pi_{0.5}$ training.

Segmenter	LIBERO Sim SR (%)					Franka Real (X/30)				
	L-10	L-Goal	L-Object	L-Spatial	Avg	T1	T2	T3	T4	Avg (%)
Uniform partition on \mathbf{G}	65.0	80.0	72.0	88.0	76.2	9/30	15/30	15/30	20/30	49.2
Spectral clustering	70.0	85.0	80.0	94.6	82.4	10/30	18/30	17/30	22/30	55.8
Agglomerative clustering	74.0	86.0	86.0	93.0	84.8	11/30	19/30	18/30	21/30	57.5
Bayesian change-point	80.0	89.0	88.0	95.0	88.0	11/30	20/30	18/30	23/30	60.0
KTS (Ours)	88.8	96.0	94.2	96.4	93.9	12/30	22/30	19/30	28/30	67.5

Video-quality details. Per-suite video quality. Tab. 10 expands the suite-averaged Tab. 2 of the main body into the four LIBERO suites. SKIP strictly wins every (suite, metric) cell. The dense Wan 2.2 baseline’s per-suite FVD spans 2768 to 6610, $3\times$ to $15\times$ higher than any sparse-anchor row on each suite, confirming that chunked recursive sampling accumulates substantial long-horizon drift that sparse keyframe generation avoids.

Table 10: **Per-suite end-to-end video quality on LIBERO test suites**. Detailed breakdown of the averaged Tab. 2 of the main body. SKIP leads on every (suite, metric) cell.

Suite	Method	PSNR \uparrow	SSIM \uparrow	LPIPS \downarrow	FVD \downarrow
LIBERO-10	Wan 2.2 (chunked)	21.373	0.833	0.176	3703
	Uniform	21.112	0.837	0.146	596
	RDP	21.004	0.836	0.149	562
	TriPSS	20.836	0.811	0.161	636
	SKIP (Ours)	21.504	0.844	0.138	548
LIBERO-Goal	Wan 2.2 (chunked)	20.819	0.826	0.160	3238
	Uniform	20.463	0.826	0.151	617
	RDP	20.479	0.825	0.153	572
	TriPSS	20.515	0.823	0.146	508
	SKIP (Ours)	20.958	0.842	0.130	468
LIBERO-Object	Wan 2.2 (chunked)	21.890	0.838	0.157	6610
	Uniform	22.085	0.877	0.098	845
	RDP	21.934	0.873	0.105	943
	TriPSS	21.787	0.831	0.147	774
	SKIP (Ours)	22.371	0.885	0.090	445
LIBERO-Spatial	Wan 2.2 (chunked)	21.525	0.833	0.157	2768
	Uniform	21.552	0.841	0.134	762
	RDP	20.759	0.831	0.146	751
	TriPSS	20.851	0.839	0.176	622
	SKIP (Ours)	21.576	0.845	0.126	393

Budget sensitivity. The keyframe budget K_{kf} controls the cost-quality trade-off of the sparse-to-dense paradigm. Lower K_{kf} saves generator inference cost but risks missing manipulation events, while higher K_{kf} approaches dense generation in cost without proportional quality gain. We sweep $K_{\text{kf}} \in \{9, 17, 33, 41, 57\}$ and report selection metrics, video quality, and downstream policy SR at each point.

Saturation curve. As shown in Fig. 7, GripCov, MEC, and OAS all enter an elbow near $K_{\text{kf}} = 41$ on LIBERO, and downstream-generator PSNR enters its elbow at the same point. The choice of $K_{\text{kf}} = 41$ thus rests on three independent criteria, namely event-coverage saturation, downstream PSNR elbow, and BIC consensus on segment count, and aligns with both the $4N+1$ and $8N+1$ frame budgets of common video diffusion backbones.

Selection and video metrics at each K_{kf} . As shown in Tab. 11, all five selection-quality metrics improve monotonically with K_{kf} up to $K_{\text{kf}} = 41$ and then plateau or slightly regress at $K_{\text{kf}} = 57$ because the selector starts emitting near-redundant keyframes. PSNR / SSIM / LPIPS follow the same elbow profile, indicating that the video generator gains less per extra keyframe past $K_{\text{kf}} = 41$.

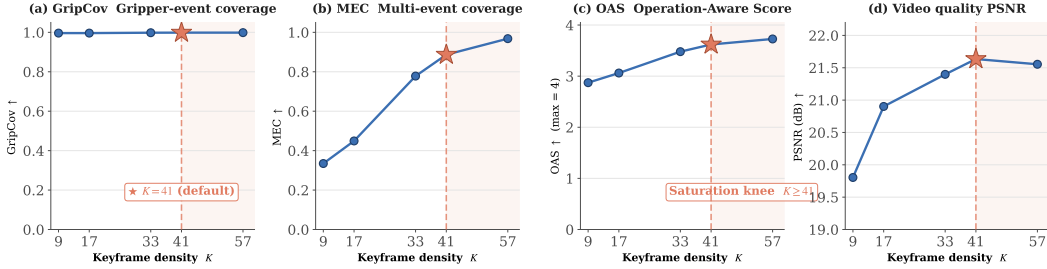


Figure 7: **Event coverage and video quality saturate near $K_{kf} = 41$.** Increasing the keyframe budget improves event coverage and downstream video quality up to the elbow near $K_{kf} = 41$. Higher budgets give smaller marginal gains while increasing inference cost.

The $K_{kf} = 33$ row remains within 0.013 OAS and 0.24 dB PSNR of $K_{kf} = 41$, suggesting that a 20% keyframe-count reduction is available with only marginal quality loss.

Table 11: **Keyframe-budget sweep: selection + video metrics.**

K_{kf}	MEC↑	GripCov↑	MaxSemDist↓	P95SemDist↓	OAS↑	PSNR↑	SSIM↑	LPIPS↓
9	0.742	0.852	0.205	0.176	0.803	19.804	0.812	0.158
17	0.818	0.934	0.165	0.142	0.861	20.902	0.832	0.139
33	0.870	0.978	0.140	0.116	0.898	21.398	0.847	0.126
41 (Ours)	0.888	0.999	0.132	0.109	0.911	21.635	0.856	0.119
57	0.882	0.998	0.137	0.113	0.908	21.554	0.852	0.123

Downstream policy SR at each K_{kf} . As shown in Tab. 12, downstream $\pi_{0.5}$ SR scales sub-linearly with K_{kf} and peaks at $K_{kf} = 41$ on both LIBERO sim (avg 93.9%) and Franka real (avg 67.5%). $K_{kf} = 57$ regresses by 0.6 pp sim and 4.2 pp real, with FVD up-ticking from 458 to 478. Past the elbow, the additional keyframes are near-redundant and dilute the generator’s fixed compute budget across less informative frames, which delivers noisier supervision to $\pi_{0.5}$. The real-robot side is more sensitive than simulation because fine-motor cues during contact-rich moments are not masked by simulator pose tolerances.

Table 12: **Keyframe-budget sweep: downstream $\pi_{0.5}$ SR (Mix100).** FVD up-tick and Real-SR drop at $K_{kf}=57$ mark diminishing returns past the elbow.

K_{kf}	LIBERO Sim SR (%)					Franka Real (X/30)					FVD↓
	L-10	L-Goal	L-Object	L-Spatial	Avg	T1	T2	T3	T4	Avg (%)	
9	67.5	81.7	75.1	85.7	77.5	10/30	16/30	14/30	20/30	50.0	712
17	76.3	88.4	86.3	95.0	86.5	11/30	19/30	17/30	23/30	58.3	568
33	87.5	93.8	92.5	96.2	92.5	11/30	21/30	18/30	27/30	64.2	489
41 (Ours)	88.8	96.0	94.2	96.4	93.9	12/30	22/30	19/30	28/30	67.5	458
57	88.0	95.4	93.6	96.2	93.3	11/30	20/30	18/30	27/30	63.3	478

Recovery diagnostics. Gap predictor accuracy under distribution shift. The gap predictor is trained on ground-truth keyframes but at full-pipeline inference it receives SKIP-GENERATOR-synthesized keyframes, which exhibit appearance drift relative to the originals. Tab. 13 measures its prediction accuracy on this shifted input. The weighted-average RMSE of 1.548 frames (MAE 1.010) corresponds to roughly 0.10 seconds of timing offset at 16 FPS. Per-suite trends mirror the end-to-end quality results, namely LIBERO-10 has the largest error (2.708-frame RMSE) and also the least stable generated-keyframe appearance, while LIBERO-Spatial has the smallest (0.779). This error magnitude has bounded impact on AC-FILM’s recursive midpoint interpolation, since the recursion distributes a single gap error across multiple subdivision levels, a partial explanation for why end-to-end SSIM remains above 0.83 on every suite except LIBERO-10.

Anchor placement on dense recovery. Fig. 8 shows a long two-object LIBERO trajectory where event-aware keyframes preserve object-in-gripper states that uniform or geometry-only anchors miss.

Table 13: **Gap predictor accuracy on SKIP-GENERATOR keyframes.** Frame-level prediction error of the gap predictor when applied to generated (rather than GT) adjacent keyframes, reflecting full-pipeline distribution shift.

Suite	RMSE (frames)↓	MAE (frames)↓
LIBERO-10	2.708	2.118
LIBERO-Goal	1.318	0.943
LIBERO-Object	1.079	0.781
LIBERO-Spatial	0.779	0.480
Weighted average	1.548	1.010

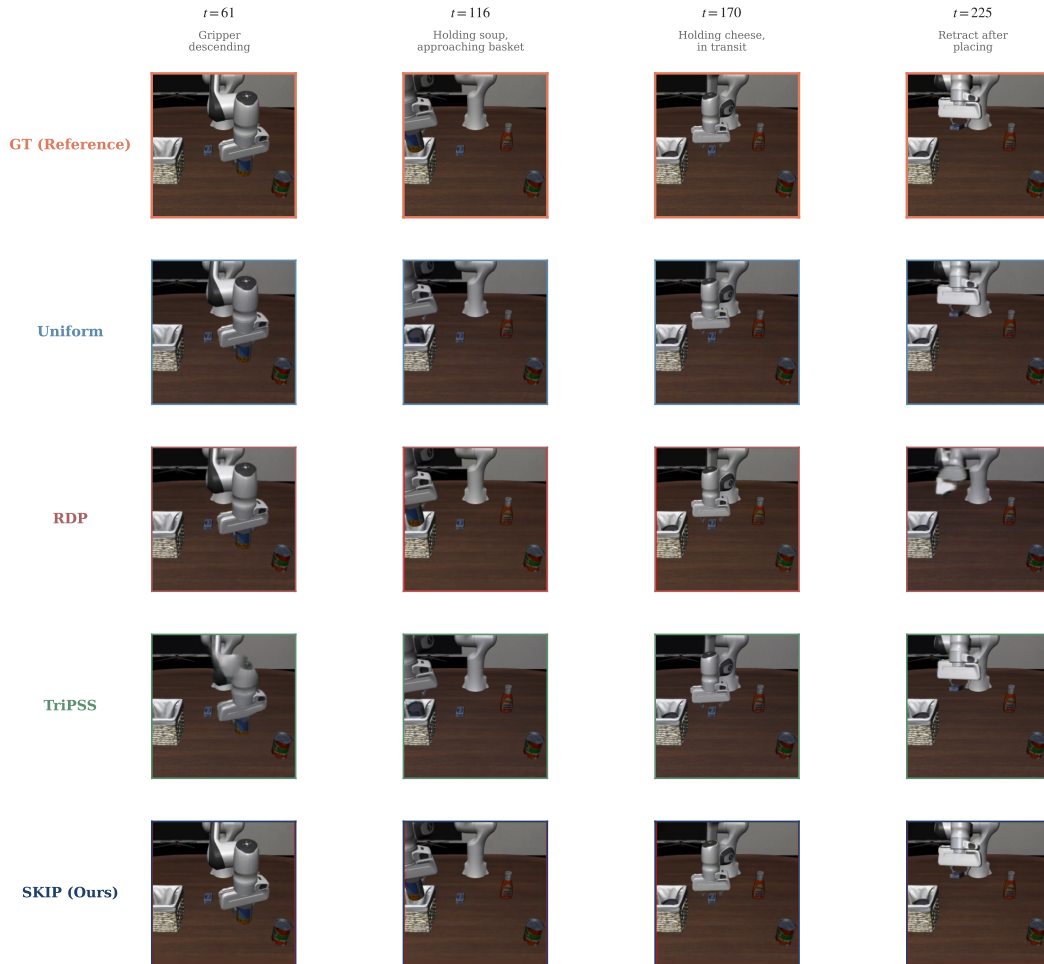


Figure 8: **Qualitative effect of keyframe placement on dense recovery.** On a long two-object LIBERO trajectory, event-aware keyframes help preserve object-in-gripper states that uniform or geometry-only anchors can miss.

Generated dense rollouts: failure modes. Fig. 9 shows two recurring failure modes in LIBERO-10’s compound tasks. The first is a *phase-switching offset* between subtasks such as opening a stove and placing a moka pot, which causes mid-trajectory object poses to drift from ground truth. The second is *end-stage degradation* on multi-step tasks such as pick-place-and-close-microwave, where the third sub-action accumulates the errors of the first two. Both modes correlate with task length and the number of sub-actions, indicating that the video generator is the residual bottleneck on long compositional rollouts.



Figure 9: **Generated dense rollouts versus ground truth.** Sampled frames from SKIP’s reconstructed rollouts (Gen) against ground-truth episodes (GT) on success and failure cases from LIBERO-10, LIBERO-Spatial, and LIBERO-Object. Failures concentrate in compound multi-stage tasks where errors near phase switches accumulate.

C.2 Policy-data extensions (§4.3)

Per-condition success rates. LIBERO simulation per-suite SR. As shown in Tab. 14, SKIP-Mix70 tracks the all-real reference within 1 pp on every LIBERO suite, and the per-suite difficulty gradient is preserved. LIBERO-10 is the hardest of the four suites under both Real (90.1%) and SKIP-Mix70 (89.6%), while LIBERO-Spatial is the easiest under both (97.9% Real vs. 97.5% SKIP-Mix70). Dense-Mix70 collapses to between 59.4 and 68.5% and Dense-Mix100 drops further to

between 35.5 and 38.6%, with the largest absolute degradation on LIBERO-10 (Real 90.1% vs. Dense-Mix100 35.5%, a 54.6 pp gap). The policy trained on SKIP videos therefore inherits the same task-difficulty profile as the all-real-trained one, while dense-generated rollouts lose information most at long-horizon, high-event-count cells.

Table 14: $\pi_{0.5}$ **success rate on LIBERO simulation** (% , per suite). Each condition uses 1503 training trajectories. Real demos (gray) is the all-real reference, and among the four synthetic-mix conditions the best per column is highlighted.

Training condition	LIBERO-10 \uparrow	LIBERO-Goal \uparrow	LIBERO-Object \uparrow	LIBERO-Spatial \uparrow	Avg. \uparrow
Real demos	90.1	96.5	96.3	97.9	95.2
SKIP-Mix70	89.6	96.6	96.0	97.5	94.9
Dense-Mix70	59.4	67.1	68.5	64.9	65.0
SKIP-Mix100	88.8	96.0	94.2	96.4	93.9
Dense-Mix100	35.5	38.4	37.7	38.6	37.5

Franka real-robot per-task SR. As shown in Tab. 15, SKIP-Mix70 matches Real demos within one success out of 30 on every real-robot task, and even slightly beats Real on T2 (26/30 vs. 25/30). Dense-Mix70 drops to between 5 and 18 successes (avg 40.8% vs. Real 74.2%) and Dense-Mix100 collapses to between 2 and 11 successes (avg 25.8%). T1 (multi-mug sequential pick-and-place) is hit hardest at 2/30, matching the long-horizon failure mode that dominates LIBERO-10 in Tab. 14. The real-robot side amplifies the SKIP-vs-Dense gap relative to simulation because the fine-motor cues that dense 49-frame chunked generation drifts on are not masked by simulator pose tolerances.

Table 15: $\pi_{0.5}$ **success rate on Franka Panda real robot**. Each cell reports successes out of 30 rollouts. Real demos (gray) is the all-real reference, and among the four synthetic-mix conditions the best per column is highlighted.

Training condition	T1 \uparrow	T2 \uparrow	T3 \uparrow	T4 \uparrow	Avg. SR (%) \uparrow
Real demos	14/30	25/30	22/30	28/30	74.2
SKIP-Mix70	14/30	26/30	21/30	27/30	73.3
Dense-Mix70	5/30	16/30	10/30	18/30	40.8
SKIP-Mix100	12/30	22/30	19/30	28/30	67.5
Dense-Mix100	2/30	10/30	8/30	11/30	25.8

T1: Put both red and blue mugs in basket. T2: Put red bowl in drawer and close drawer.
T3: Put white mug on plate. T4: Stack red bowl on green bowl.

Cross-method downstream comparison. To complete the cross-method comparison initiated at the selection-quality level (Tab. 1 and Tab. 7), we run each baseline selection method through the full SKIP pipeline. Its selected keyframes feed SKIP-GENERATOR, then SKIP-RECONSTRUCTOR, and the resulting synthetic videos train $\pi_{0.5}$ under identical Mix70 and Mix100 protocols to the SKIP-Mix conditions.

Aggregate cross-method SR. As shown in Tab. 16, SKIP-Mix70 outperforms every baseline-Mix70 counterpart by between 7.5 (vs. RDP) and 13.9 pp (vs. TriPSS) in simulation, and by between 15.0 and 23.3 pp on the real robot. At Mix100 the gap widens further by an additional 7.2 to 8.3 pp in simulation and 2.5 to 3.3 pp on the real robot, because the real-data buffer in Mix70 partially compensates for weaker selection. The cross-method ranking by SR (SKIP > RDP > Uniform > TriPSS) follows the OAS ranking from Tab. 1, confirming that selection quality is decisive at the policy-training level.

Cross-method per-suite LIBERO breakdown. As shown in Tab. 17, the SKIP-Mix70-vs-baseline gap is largest on LIBERO-10 (the most event-dense suite in Tab. 14), where SKIP-Mix70 reaches 89.6% versus 80.0% for RDP-Mix70, 75.0% for Uniform-Mix70, and 67.0% for TriPSS-Mix70. The gap shrinks on LIBERO-Spatial where all four methods exceed 90% at Mix70 because spatial tasks are short-horizon with few gripper events. This per-suite pattern shows that baseline selectors lose ground exactly on the suites that demand event-aware keyframing, which is where SKIP-SELECTOR’s gripper-event protection contributes most.

Table 16: **Cross-method downstream: aggregate $\pi_{0.5}$ success rate.**

Method	Mix	OAS \uparrow	LIBERO Sim Avg (%)	Franka Real Avg (%)
Real demos (reference)	n/a	n/a	95.2	74.2
Uniform-Mix70	70	0.825	84.8	54.2
Uniform-Mix100	100	0.825	75.8	45.8
RDP-Mix70	70	0.848	87.4	58.3
RDP-Mix100	100	0.848	79.2	49.2
TriPSS-Mix70	70	0.787	81.0	50.0
TriPSS-Mix100	100	0.787	71.7	41.7
SKIP-Mix70 (Ours)	70	0.911	94.9	73.3
SKIP-Mix100 (Ours)	100	0.911	93.9	67.5

Table 17: **Cross-method downstream: per-suite LIBERO Sim SR.** Per-suite breakdown of Tab. 16.

Method (Mix)	LIBERO-10 \uparrow	LIBERO-Goal \uparrow	LIBERO-Object \uparrow	LIBERO-Spatial \uparrow	Avg \uparrow
Real demos (reference)	90.1	96.5	96.3	97.9	95.2
Uniform-Mix70	75.0	86.5	84.0	93.7	84.8
Uniform-Mix100	67.0	78.0	72.0	86.0	75.8
RDP-Mix70	80.0	87.0	88.0	94.6	87.4
RDP-Mix100	71.0	78.0	77.5	90.3	79.2
TriPSS-Mix70	67.0	82.0	85.0	90.0	81.0
TriPSS-Mix100	58.0	71.0	80.0	77.8	71.7
SKIP-Mix70 (Ours)	89.6	96.6	96.0	97.5	94.9
SKIP-Mix100 (Ours)	88.8	96.0	94.2	96.4	93.9

Cross-method per-task real-robot breakdown. As shown in Tab. 18, the per-task pattern mirrors the per-suite finding above. SKIP-Mix70’s lead is widest on T1 (14/30 vs. between 10 and 13/30 for baselines) and T4 (27/30 vs. between 18 and 22/30), the two longest-horizon real-robot tasks. T2 and T3 (shorter, fewer events) show smaller gaps, consistent with selection quality mattering less when manipulation events are sparse. At Mix100 the SKIP-Mix advantage on T1 holds up at 12/30 versus best baseline 11/30, reproducing the long-horizon resilience seen in LIBERO-10 of Tab. 17.

Table 18: **Cross-method downstream: per-task Franka real-robot SR.** Per-task breakdown of Tab. 16, 30 rollouts per task.

Method (Mix)	T1 \uparrow	T2 \uparrow	T3 \uparrow	T4 \uparrow	Avg SR (%) \uparrow
Real demos (reference)	14/30	25/30	22/30	28/30	74.2
Uniform-Mix70	13/30	17/30	16/30	19/30	54.2
Uniform-Mix100	10/30	15/30	13/30	17/30	45.8
RDP-Mix70	13/30	18/30	17/30	22/30	58.3
RDP-Mix100	11/30	15/30	14/30	19/30	49.2
TriPSS-Mix70	10/30	17/30	14/30	19/30	50.0
TriPSS-Mix100	8/30	14/30	12/30	16/30	41.7
SKIP-Mix70 (Ours)	14/30	26/30	21/30	27/30	73.3
SKIP-Mix100 (Ours)	12/30	22/30	19/30	28/30	67.5

C.3 Ablation extensions (§4.4)

Intermediate selection and recovery metrics. Tab. 19 reports the keyframe-quality and dense-recovery metrics that the downstream success rates of Tab. 4 aggregate, so we can trace which design choice contributes to which SR delta. In panel (a), the proprioceptive stream alone reaches OAS 0.880 and is the strongest single modality, ahead of V (0.795) and S (0.683), reflecting that proprio captures contact events that vision struggles to localize. Adding gripper-event post-processing on top of full V+S+P fusion lifts GripCov from 0.842 to 0.999 and OAS from 0.863 to 0.911, the largest single-step gain in the table. In panel (b), action conditioning lifts dense-recovery PSNR by +0.730 dB, SSIM by +0.008, and LPIPS by -0.005 under identical SKIP-Selector keyframes (paired t -test $p < 0.01$), confirming that the AC-FILM modulation rather than the keyframe selection is what improves the per-frame fidelity of the recovered rollout.

OAS validity check. Since OAS is a custom keyframe-quality metric, we verify that it tracks downstream policy performance. We pair the OAS values from Tab. 19(a) with the corresponding $\pi_{0.5}$ success rates from Tab. 4 (six selection ablations with action conditioning fixed to AC-FILM),

Table 19: **Ablations on LIBERO test suites.** Left: modality and gripper-event post-processing ablation for keyframe selection. Right: action conditioning ablation for dense recovery under identical SKIP-Selector keyframes.

(a) Keyframe selection (AC fixed to AC-FILM)						(b) Dense recovery (V/S/P/PP fixed to Ours)			
V	S	P	PP	GripCov \uparrow	OAS \uparrow	AC	PSNR \uparrow	SSIM \uparrow	LPIPS \downarrow
✓	✗	✗	✗	0.729	0.795	✗	30.310	0.969	0.028
✗	✓	✗	✗	0.396	0.683	✓	31.040	0.977	0.023
✗	✗	✓	✗	0.921	0.880	Δ	+0.730	+0.008	-0.005
✓	✓	✗	✗	0.668	0.788				
✓	✓	✓	✗	0.842	0.863				
✓	✓	✓	✓	0.999	0.911				

Paired t -test $p < 0.01$.

and add the three cross-method points (Uniform, RDP, TriPSS feeding SKIP-GENERATOR under Mix70) from Tab. 16. Fig. 10 shows the resulting scatter on both LIBERO simulation and the Franka real robot ($N=9$ for each panel). The Spearman rank correlations are $\rho = 0.67$ on LIBERO sim and $\rho = 0.72$ on Franka real, and the Pearson correlations are $r = 0.70$ ($p < 0.05$) on LIBERO sim and $r = 0.83$ ($p < 0.01$) on Franka real. The consistent monotonic relationship across two evaluation regimes supports OAS as a meaningful proxy for downstream policy gain.

OAS vs. downstream $\pi_{0.5}$ success rate

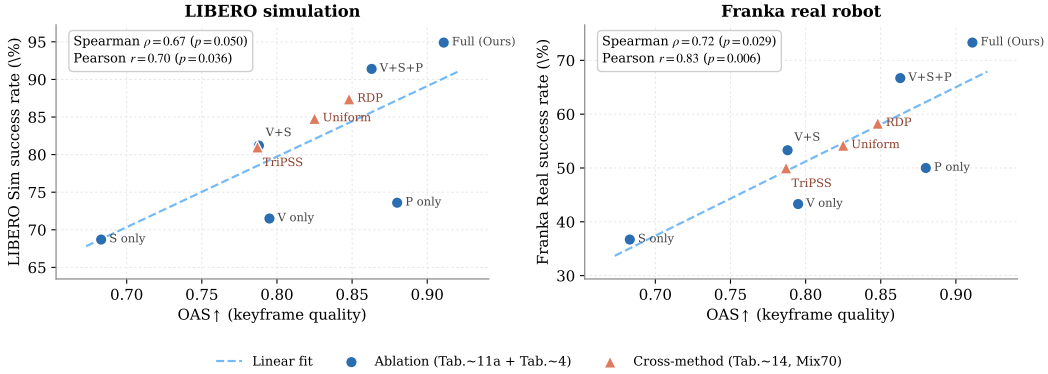


Figure 10: **OAS tracks downstream $\pi_{0.5}$ success rate.** Circle markers are the six selection-ablation configurations from Tab. 19(a) paired with their downstream success rates from Tab. 4 (action conditioning fixed to AC-FILM). Triangle markers are the three cross-method points (Uniform / RDP / TriPSS feeding SKIP-GENERATOR under the Mix70 protocol) from Tab. 16. Dashed line is a linear fit across all nine points.

Fusion-weight ablation. As shown in Tab. 20, equal weighting reaches OAS 0.911 and wins by a small margin over effective-rank-weighted (0.903) and fixed-weight (0.4/0.4/0.2, 0.900). Grid search, despite being more sophisticated, scores the lowest at 0.863 because per-suite weights overfit to the validation split. Looking at the sub-metric breakdown, GripCov stays at 0.999 across all four strategies because gripper-event post-processing guarantees coverage regardless of fusion weighting. The OAS spread is therefore driven mainly by MEC (0.888 for Equal vs. 0.800 for Grid search) and the two semantic-span metrics (MaxSemDist 0.132 \rightarrow 0.190, P95SemDist 0.109 \rightarrow 0.157), confirming that fusion weighting affects multi-event coverage and visual-semantic span but not gripper-event coverage. The narrow 0.011 OAS gap between equal weighting and the two structured alternatives further indicates that the centering and trace-normalization step already brings the three modalities to comparable scale, so equal weighting is both the simplest and the strongest choice in this regime.

Table 20: Fusion-weight ablation on SKIP-SELECTOR.

Fusion strategy	MEC \uparrow	GripCov \uparrow	MaxSemDist \downarrow	P95SemDist \downarrow	OAS \uparrow
Equal weighting	0.888	0.999	0.132	0.109	0.911
Effective-rank-weighted	0.875	0.999	0.145	0.117	0.903
Fixed (0.4/0.4/0.2)	0.870	0.999	0.149	0.120	0.900
Grid search	0.800	0.999	0.190	0.157	0.863

Generative AI usage disclosure. We used large language models (Claude Opus 4.7 and GPT-5.5) for two purposes. For *writing assistance*, they provided grammar correction, style editing, and paraphrasing while polishing an originally Chinese manuscript into English. For *code generation and debugging*, they helped draft and debug the figure-generation and data-analysis scripts. All research ideas, technical content, experimental data, and analyses were produced and verified by the authors.